Modeling Nonclassical Heterogeneous Bubble Nucleation from Cellulose Fibers: Application to Bubbling in Carbonated Beverages

Gérard Liger-Belair,* Cédric Voisin, and Philippe Jeandet

Laboratoire d'Œnologie et de Chimie Appliquée, UPRES EA 2069, URVVC, Faculté des Sciences de Reims, Moulin de la Housse, B.P. 1039, 51687 Reims, Cedex 2, France

Received: April 1, 2005; In Final Form: June 2, 2005

In this paper, the kinetics of CO_2 bubble nucleation from tiny gas pockets trapped inside cellulose fibers immersed in a glass of champagne were investigated, in situ, from high-speed video recordings. Taking into account the diffusion of CO_2-dissolved molecules from the liquid bulk to the gas pocket, a model was derived which enabled us to connect the kinetics of bubble nucleation with both fiber and liquid parameters. Convection was found to play a major role in this process. The boundary layer around the gas pocket where a gradient of CO_2-dissolved molecules exists was also indirectly approached and found to be in the order of $10-20\ \mu$m. Because most of the particles adsorbed on the wall of a container or vessel free from any particular treatment are also believed to be cellulose fibers coming from the surrounding air, the results of this paper could be indeed extended to the more general field of nonclassical heterogeneous bubble nucleation from supersaturated liquids.

1. Introduction

During the past decades, there has been a large body of research concerning the nucleation of bubbles from liquids, being for example bubbles emerging from a heated plane, bubbles formed at the tip of an immersed blowing nozzle, cavitation bubbles imploding on a propeller surface, or bubbles spontaneously born in the liquid bulk by homogeneous nucleation.[1−4] Nevertheless, only quite recently, much interest was devoted to the formation of bubbles in sparkling beverages.[5−7]

Sparkling beverages are supersaturated with CO_2-dissolved gas molecules. Actually, as soon as a liquid medium is supersaturated with dissolved gas molecules, the bulk free energy per unit of volume, Δg_V, associated with the transfer of dissolved gas molecules into the vapor phase is negative, and therefore thermodynamically favorable. However, the bubble production process also results in the production of interfacial free energy. Below a critical radius, $r_C = -2\gamma/\Delta g_V$, where γ is the surface tension of the liquid medium, the bubble embryo formation results in a net increase of the total free energy of the system. Henceforth, classical nucleation is characterized by an energy barrier to overcome.

Most of the bubble nucleation sites in glasses poured with a sparkling beverage were recently found to be located on preexisting gas cavities trapped inside hollow and roughly cylindrical-like cellulose fibers, cast off from paper or cloth which floated from the surrounding air and/or remaining from the dry wiping process.[8−10] Actually, in weakly carbonated liquids such as carbonated beverages in general, carbon dioxide bubble formation necessarily requires preexisting immersed gas cavities with radii of curvature larger than the above-defined critical radius, to overcome the nucleation energy barrier and grow freely.[11,12] Jones et al. made a classification of the broad range of nucleation likely to be encountered in liquids supersaturated with dissolved gas.[13] Bubble formation from preexisting gas cavities larger than the critical size is referred to as nonclassical heterogeneous bubble nucleation (type IV bubble nucleation, following their nomenclature[13]). The hollow cavity within the fiber where the preexisting gas pocket gets trapped is denoted the *lumen*.

In this paper, the conditions of entrapment of a tiny gas pocket inside a fiber's lumen are examined as well as its dynamics through the lumen driven by the diffusion of CO_2-dissolved molecules from the liquid bulk.

2. Experimental Section

2.1. Material. A standard commercial champagne wine was poured in a classical crystal flute first rinsed using distilled water and then air-dried. Some physicochemical parameters of champagne were already determined at 20 °C, with a sample of champagne first degassed.[8] The static surface tension of champagne, γ, was found to be of the order of 47 mN m^{-1}, its density, ρ, was measured and found to be 998 kg m^{-3}, and its dynamic viscosity, η, was found to be of the order of 1.5×10^{-3} kg m^{-1} s^{-1}. Therefore, the capillary length of champagne is $(\gamma/\rho g)^{1/2} \approx 2$ mm, where g is the gravity acceleration. In a previous work, the carbon dioxide dissolved into the liquid matrix was also accurately measured with an imaging spectrometer by use of the ^{13}C magnetic resonance spectroscopy (MRS) technique as an original unintrusive and nondestructive method.[14] Typically, champagne holds about 10 g/L of CO_2-dissolved molecules.

2.2. Setup. The dynamics of bubble nucleation were captured with a high-speed digital video camera (Speedcam+, Vannier Photelec, Antony, France) able to film up to 2000 frames/s and fitted with a microscope objective (Mitutoyo, M Plan Apo 5, Japan). The champagne was first poured into the flute, which was placed between the objective and a cold source light (Fiber-Lite, PL-900, DC regulated illuminator). A photograph of the whole workbench is displayed in Figure 1A together with the typical shadowgraph image of a cellulose fiber acting as a bubble nucleation site in Figure 1B.

3. Results and Discussion

3.1. Entrapping a Gas Pocket inside a Fiber. Cellulose fibers are in the form of hollow tubes of several hundreds of

* Corresponding author. Phone: (33)3 26 91 86 14. Fax: (33)3 26 91 33 40. E-mail: gerard.liger-belair@univ-reims.fr.

10.1021/jp051650y CCC: $30.25
Published on Web 07/13/2005

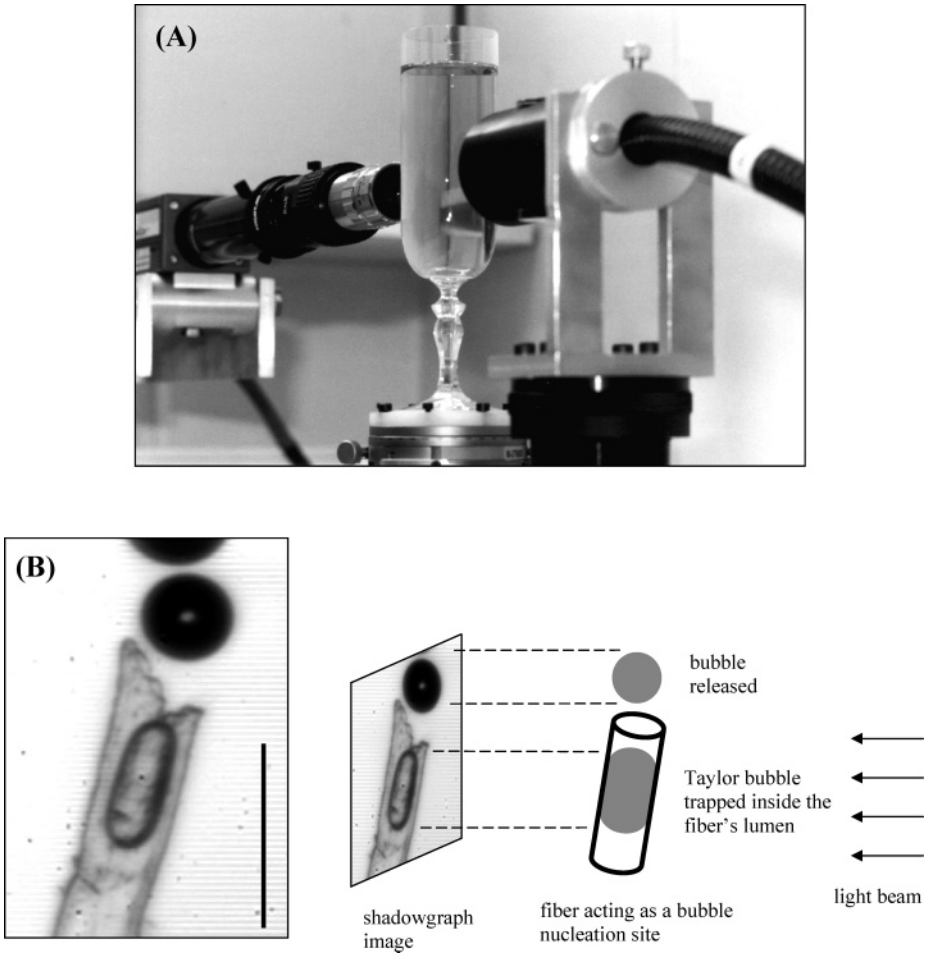

Figure 1. Photographic detail of the workbench used to observe in situ the nucleation of bubbles from cellulose fibers found on the glass wall (A). The gas pockets trapped inside the fiber's lumen and responsible for the repetitive production of bubbles clearly appear in dark (B). Bar = 50 μm.

micrometers long and with a cavity mouth of several micrometers wide. The central cavity within the fiber is denoted as the lumen. The fiber wall section consists of densely packed cellulose microfibrils, with a preferential orientation along the fiber axis. Cellulose microfibrils consist of glucose units bounded in a β-conformation favoring straight polymer chains. The different structural levels of a cellulose fiber are presented in Figure 2. For a current review on the molecular and supramolecular structures of cellulose, see the article by O'Sullivan[15] and references therein.

From the physics point of view, cellulose fibers can indeed be considered as tiny, roughly cylindrical capillary tubes of radius r and length h. Consequently, a wetting liquid placed in contact with this highly hydrophilic material penetrates it by capillary action. Actually, in capillaries with radii much smaller than the capillary length, gravity may be neglected. Therefore, with z being the distance of penetration at time t, the overall balance of forces on the liquid in the capillary may be expressed as

$$\rho\left[z\frac{\mathrm{d}^2z}{\mathrm{d}t^2}+\left(\frac{\mathrm{d}z}{\mathrm{d}t}\right)^2\right]=\frac{2\gamma\cos\varphi}{r}-\frac{8\eta z}{r^2}\frac{\mathrm{d}z}{\mathrm{d}t} \qquad (1)$$

where φ is the angle between the liquid and the capillary wall. The left-hand side of the latter equation is related to the liquid inertia, whereas both terms on the right-hand side are related to capillarity (the driving force) and viscous resistance, respectively.

Under steady conditions, capillarity is balanced by the viscous drag of the liquid, and the famous Lucas−Washburn equation

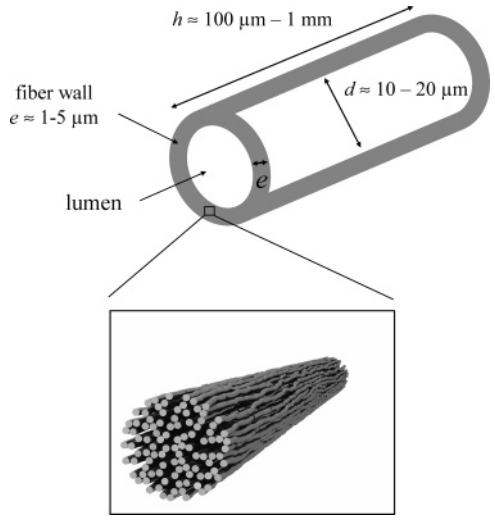

Figure 2. The different structural levels of a typical cellulose fiber. The fiber wall consists of closely packed cellulose microfibrils oriented mainly in the direction of the fiber.[15]

can be derived, which relates the distance of penetration, z, at time t to the wetting properties of the capillary and the viscosity of the liquid:[16,17]

$$z^2=\frac{r\gamma\cos\varphi}{2\eta}t \qquad (2)$$

Let's imagine a liquid edge spreading with a velocity, v, along a solid surface where cellulose fibers are adsorbed. This is

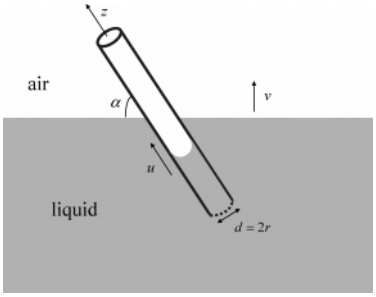

Figure 3. From the physics point of view, a fiber may be seen as a tiny capillary tube which gets invaded by a wetting liquid placed into contact with one of the fiber's tips; v is the velocity of the liquid edge advancing over the fiber, and u is the velocity at which the meniscus advances inside the fiber's lumen by capillary action.

basically what happens when a glass is filled with a liquid. Actually, during the pouring process, a liquid edge progressively advances along the vertical glass wall at a velocity, v, of the order of several centimeters per second. As soon as the wetting liquid comes into contact with the fiber, some liquid progressively penetrates and fills the fiber's lumen by capillary rise. Finally, a gas pocket may be trapped inside the fiber's lumen if the time, τ, taken by the liquid to completely fill the lumen by capillary rise overcomes the characteristic time, T, taken to completely submerge the fiber inside the liquid (see Figure 3).

By retrieving eq 2 with the characteristic fiber's parameters defined in Figure 2, the characteristic time required to completely fill the fiber's lumen by capillary action may be expressed as

$$\tau = \frac{2\eta h^2}{r\gamma \cos \varphi} \tag{3}$$

Considering a fiber with a length, h, inclined by an angle, α, with regard to the liquid edge advancing over it at a velocity, v (see Figure 3), leads to the following time required for the fiber to be completely submerged:

$$T = \frac{h \sin \alpha}{v} \tag{4}$$

The condition of gas entrapment inside the fiber therefore is expressed as $\tau > T$, that is,

$$\frac{2\eta h^2}{r\gamma \cos \varphi} > \frac{h \sin \alpha}{v} \tag{5}$$

Because cellulose fibers are a highly hydrophilic material, the contact angle of an aqueous liquid on it is relatively small (about 30° with pure water). Consequently, $\cos \varphi \approx 1$. Finally, the condition of entrapment may be rewritten as follows:

$$\frac{h}{r \sin \alpha} > \frac{\gamma}{2\eta v} \tag{6}$$

with the geometric parameters of the cellulose fiber lying on the left-hand side of eq 6 and the liquid parameters lying on the right-hand side of eq 6.

The entrapment of an air pocket inside the lumen of a fiber during the filling of a glass is therefore favored by the following conditions, depending on both the fiber and liquid parameters: (i) fibers as elongated as possible (h long), (ii) fibers with a narrow lumen (r small), (iii) fibers as horizontal as possible with regard to the liquid edge (i.e., $\sin \alpha$ small), (iv) liquids with a small surface tension, γ, (v) liquids with a high viscosity, η, and finally (vi) a high velocity for the liquid edge advancing along the glass wall. It is worth noting that both conditions iv and v imply that hydroalcoholic carbonated beverages are more favorable than fizzy waters to entrap air pockets inside cellulose fibers during the pouring process. Actually, the surface tension of champagne and beer is in the order of 45 mN/m (i.e., about 30 mN/m less than the surface tension of pure water), and their dynamic viscosity is about 50% higher than that of pure water.[8] Figure 4 illustrates the condition of entrapment displayed in eq 6. Figure 4 was built with the numerical values of the champagne surface tension and kinematic viscosity and with a liquid edge advancing at a reasonable velocity, v, of 5 cm/s, that is, approximately 2 s to fill a glass.

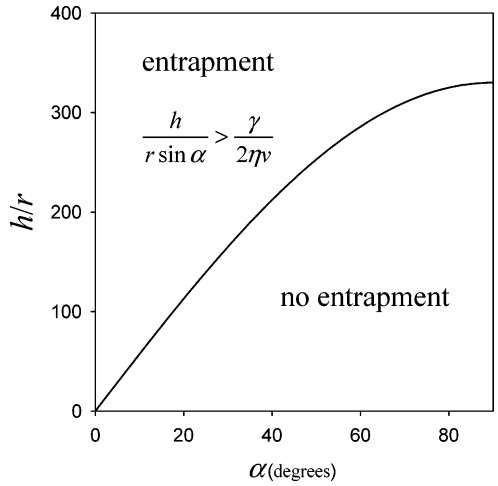

Figure 4. Conditions of gas pocket entrapment given by the ratio of the fiber's length to the fiber's radius of aperture as a function of angle α; to entrap a gas pocket inside a fiber's lumen, the ratio h/r must be fulfilled in eq 6.

Figure 5. A curve-shaped fiber naturally increases the time taken by the liquid to fully invade the fiber's lumen. Bar = 50 μm.

Remember that this model considers fibers as straight capillary tubes. It is worth noting that real fibers are nevertheless often curved, which certainly increases the likelihood of air entrapment when pouring, by increasing the time, τ, required for the liquid to completely invade the fiber's lumen by capillary action during the full immersion of the fiber (see, for example, the fiber displayed in Figure 5).

3.2. Gas Pocket's Dynamics inside the Fiber's Lumen as Observed from High-Speed Video Recordings. A typical time sequence illustrating one period of the cycle of bubble production from a typical cellulose fiber is displayed in Figure 6. The gas pocket trapped inside the fiber's lumen strikingly resembles, in miniature, a Taylor-like bubble trapped inside a microchannel.

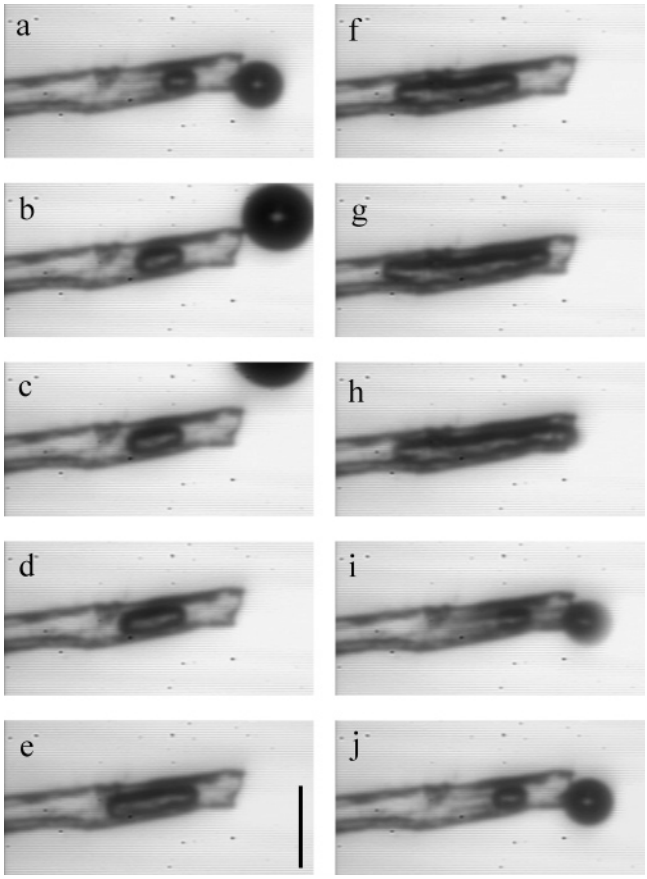

Figure 6. Time sequence illustrating one period of the cycle of bubble production from a typical cellulose fiber adsorbed on the wall of a glass poured with champagne; from frame a to frame h, the time interval between each frame is about 100 ms, whereas it is only about 1 ms between frame h and i and also 1 ms between frame i and j. Bar = 50 μm.

Plunged into a liquid supersaturated with dissolved gas molecules, the gas pocket surface acts as a nucleation area. Gas molecules dissolved into the liquid matrix therefore diffuse inside the trapped gas pocket through the gas/liquid interface. In turn, the trapped gas pocket grows inside the fiber's lumen until it reaches a fiber's tip (from part a to part h of Figure 6). As the gas pocket reaches the tip of the fiber, a tiny bubble is ejected, but a portion of the gas pocket remains trapped inside the fiber, and shrinks back to its initial position, and the cycle starts again until bubble production stops through lack of dissolved gas molecules (from part h to part j of Figure 6). The whole process leading to the production of a bubble can be coarsely divided in two main steps: (i) the growth of the gas pocket trapped inside the fiber's lumen and (ii) the bubble detachment as the gas pocket reaches the fiber's tip. Actually, the time scale of the bubble detachment is small ($\approx$1 ms) compared with the relatively slow growth of the gas pocket (several tens to several hundreds of milliseconds). Therefore, the cycle of bubble production seems to be largely governed by the growth of the gas pocket trapped inside the fiber's lumen.

3.3. Modeling the Bubble Dynamics inside the Fiber's Lumen. To go further with the dynamics of a gas pocket growing trapped inside the lumen of a fiber, a theoretical model has to be developed. Actually, those elongated gas pockets trapped inside the lumen of cellulose fibers are bounded by two hemispherical gas/liquid interfaces of radius r, in contact with the liquid bulk inside the fiber (both ends of the gas pocket), and by a nearly cylindrical border of radius r and length z, in contact with the fiber inner wall. A scheme is displayed in Figure 7, where the geometrical parameters of this growing Taylor-like bubble are defined.

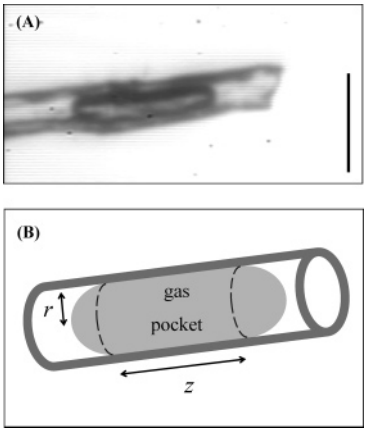

Figure 7. Real gas pocket trapped inside the lumen of a cellulose fiber acting as a bubble nucleation site in a glass poured with champagne (A), modeled as a slug-bubble trapped inside an ideal cylindrical microchannel and being fed with CO_2-dissolved molecules diffusing (i) directly from the liquid bulk through both ends of the gas pocket and (ii) through the wall of the microchannel (B). Bar = 50 μm.

Molecular diffusion is the mechanism behind the bubble growth, and the number of moles of CO_2 that cross the gas pocket interface per unit of time is ruled by

$$\frac{dN}{dt} = \iint_{\substack{\text{gas pocket}\\ \text{surface}}} \vec{J} \times d\vec{S} \tag{7}$$

where $\vec{J}$ is the flux of CO_2 molecules defined by the first Fick law, $\vec{J} = D \times \nabla\vec{c}$. In the latter equation, D is the diffusion coefficient of CO_2 molecules and $\nabla\vec{c}$ is the gradient of CO_2-dissolved molecules between the liquid bulk and the boundary layer in equilibrium with the CO_2 gas molecules in the vapor phase inside the gas pocket.

Assuming the gas in the trapped gas pocket is an ideal gas and assuming a nearly constant section ($\approx\pi r^2$) for the cylindrical body of the gas pocket, the rate at which the Taylor-like bubble grows inside the fiber's lumen, dz/dt, may be linked to the number of moles of CO_2, dN/dt, that cross the gas pocket interface through

$$\frac{dz}{dt} = \frac{\mathcal{R}\theta}{P_B \pi r^2}\frac{dN}{dt} \tag{8}$$

where $\mathcal{R}$ is the ideal gas constant, θ is the absolute temperature, and P_B is the pressure inside the gas pocket.

Actually, there are two ways in which CO_2 molecules can diffuse toward the gas pocket: (i) through the two nearly spherical caps directly in contact with the liquid bulk and (ii) through the cylindrical border in contact with the fiber wall. The diffusion coefficient of CO_2 molecules diffusing through the spherical caps is denoted as D_0, whereas that of CO_2 molecules diffusing through the fiber wall (and therefore perpendicular to the cellulose microfibrils) is denoted as $D_\perp$. D_0 is the diffusion coefficient of CO_2 molecules in the liquid bulk. It was recently measured by NMR techniques in various carbonated beverages.[14,18] In champagne, it was found to be $D_0 \approx 1.4 \times 10^{-9}$ m^2 s^{-1}, at 20 °C.[18] Very recently,[10] the transversal diffusion coefficient, $D_\perp$, of CO_2 molecules through the fiber wall was approached and properly bounded by $D_\perp/D_0 \approx 0.1$ and $D_\perp/D_0 \approx 0.3$. For modeling purposes, an intermediate value of about $D_\perp \approx 0.2D_0$ was proposed and will be used

hereafter.[10] By taking into account the two different ways in which CO_2 molecules can diffuse and because there are two spherical caps, eq 7 may be rewritten as follows:

$$\frac{dN}{dt} = \frac{dN_{SC}}{dt} + \frac{dN_{FW}}{dt} = 2 \iint_{\text{spherical cap}} \vec{J}_{SC} \times d\vec{S} + \iint_{\text{fiber wall}} \vec{J}_{FW} \times d\vec{S} \quad (9)$$

where the subscripts SC and FW correspond to the spherical cap gas/liquid interface and fiber wall, respectively.

Geometrically, the whole surface of the two spherical caps is $S_{SC} \approx 4\pi r^2$, whereas that of the cylindrical border in contact with the fiber wall is $S_{FW} \approx 2\pi rz$. Finally, by assuming the flux of CO_2 molecules is constant along each given surface and by assuming a linear gradient of CO_2 concentration in the boundary layer around the gas pocket, eq 9 may be transformed into:

$$\frac{dN}{dt} = \frac{dN_{SC}}{dt} + \frac{dN_{FW}}{dt} \approx 4\pi r^2 D_0 \frac{\Delta c}{\lambda_{SC}} + 2\pi rz D_\perp \frac{\Delta c}{\lambda_{FW}} \quad (10)$$

where λ is the boundary layer thickness and $\Delta c = c_L - c_B$ (the driving force responsible for the diffusion of CO_2 into the rising bubble) is the difference in CO_2-dissolved concentrations between the liquid bulk, denoted c_L, and the close vicinity of the bubble surface in equilibrium with the gaseous CO_2 in the gas pocket, denoted c_B.

Finally, by combining eq 10 with eq 8, the rate at which the Taylor-like bubble grows inside the fiber's lumen may be rewritten as follows:

$$\frac{dz}{dt} \approx \frac{2\mathscr{R}\theta\Delta c}{P_B}\left[\frac{D_\perp}{r\lambda_{FW}}z + \frac{2D_0}{\lambda_{SC}}\right] \quad (11)$$

Actually, in the close vicinity of the bubble surface, the CO_2-dissolved concentration, c_B, is forced by the partial pressure of gaseous CO_2 molecules inside the bubble and Henry's law locally applies, that is, $c_B = k_H P_B$, where k_H is the Henry's law constant (strongly temperature dependent). Strictly speaking, the pressure, P_B, inside the Taylor-like bubble is the sum of three terms: (i) the atmospheric pressure, P_0, (ii) the hydrostatic pressure, ρgH, with H being the depth at which the cellulose fiber lies, and (iii) the Laplace pressure, $2\gamma/r$, originating in the bubble's curvature. However, with H varying from several millimeters to several centimeters, the contribution of hydrostatic pressure is clearly negligible in front of both atmospheric and Laplace pressures. Thus, $c_B = k_H P_B \approx k_H(P_0 + 2\gamma/r)$. Finally, the only parameters unknown in eq 11 are λ_{SC} and λ_{FW}, the boundary layer thicknesses around the spherical caps and the fiber wall, respectively. The aim of the two following paragraphs is to discuss around how to approach λ_{SC} and λ_{FW}.

3.4. Pure Diffusion without Convection. Generally speaking, in a stagnant medium, heat and mass transfer are ruled by pure diffusion. In the present situation, in a purely diffusive case, each CO_2 molecule which diffuses through the gas/liquid interface into the gas pocket is removed from the boundary layer around it. In turn, the thickness of the boundary layer depleted with CO_2-dissolved molecules progressively expands around the gas pocket during the diffusing process. Due to the cylindrical shape of the gas pocket trapped inside the fiber's lumen, the boundary layer depleted with CO_2 along the cylindrical fiber wall is a cylindrical "sleeve" of liquid with a thickness of λ_{FW}. Contrary to the CO_2 molecules diffusing through the fiber wall, the CO_2 molecules diffusing through the two spherical bubble caps are removed from a nearly spherical zone of radius λ_{SC} expanding around the fiber's tips. Figure 8 illustrates the shapes taken by the boundary layers around an ideal cellulose fiber, in the purely diffusive case.

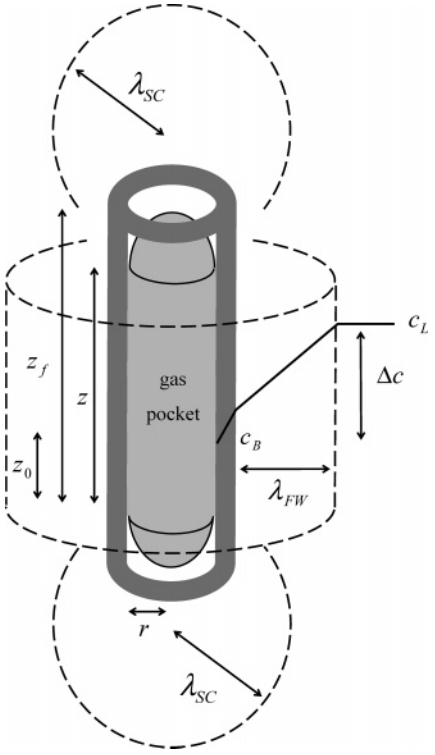

Figure 8. Sketch of the Taylor-like bubble growing trapped inside the cellulose fiber's lumen. The dashed-line limited zones are the boundary layers depleted with CO_2-dissolved molecules and where a gradient of dissolved molecules exists because of the pure diffusion of CO_2 molecules from the liquid bulk to the Taylor-like bubble.

By use of mass conservation between the boundary layer and the gas pocket, λ_{SC} and λ_{FW} may be approached. Actually, by considering the two above-defined geometries for the boundary layers, the mass conservation of CO_2 molecules between the boundary layer and the gas pocket during the diffusive process may be written as

$$\begin{cases} 8\pi\lambda_{SC}^2\, d\lambda_{SC}\, \Delta c \approx dN_{SC} \\ 2\pi(r + \lambda_{FW})z\, d\lambda_{FW}\, \Delta c \approx dN_{FW} \end{cases} \quad (12)$$

Then, by inserting the two above-mentioned expressions for dN_{SC} and dN_{FW} into eq 10 and by integrating, the growth of $\lambda_{SC}(t)$ and $\lambda_{FW}(t)$ may be deduced as time proceeds as follows:

$$\begin{cases} \lambda_{SC} \approx (2D_0 r^2 t)^{1/4} & \\ \lambda_{FW} \approx (2D_\perp t)^{1/2} & \text{for short times, i.e., } \lambda_{FW} \ll r \\ \lambda_{FW} \approx (3D_\perp rt)^{1/3} & \text{for long times, i.e., } \lambda_{FW} \gg r \end{cases} \quad (13)$$

Thus, as time goes on, a zone depleted with CO_2 progressively expands around the Taylor-like bubble which continuously consumes CO_2-dissolved molecules while releasing newly created bubbles. Consequently, as time goes on, the period required for the fiber's tip to release a bubble should inexorably increase compared with the period required to release the preceding bubble, which was clearly not observed during the clockwork release of more than 200 successive bubbles from the fiber displayed in Figure 6.

3.5. When Convection Plays Its Part. Actually, the liquid around the fiber is far from stagnant mainly due to bubbles

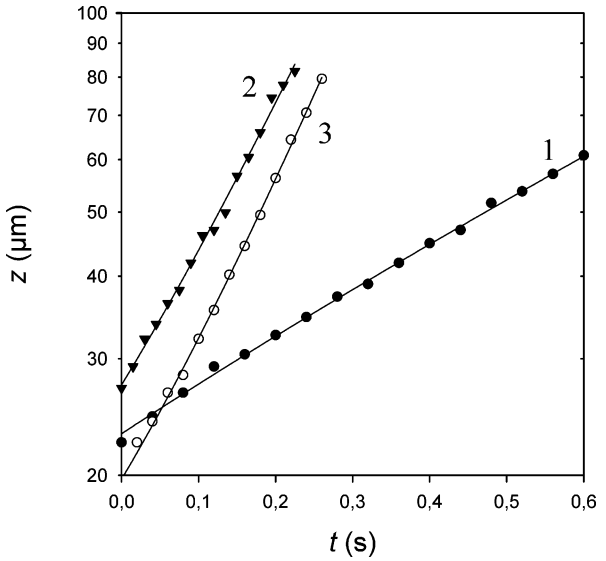

Figure 9. For the three investigated Taylor-like bubbles growing trapped inside their corresponding lumen, bubbles' lengths plotted versus time during one period of the cycle of bubble production.

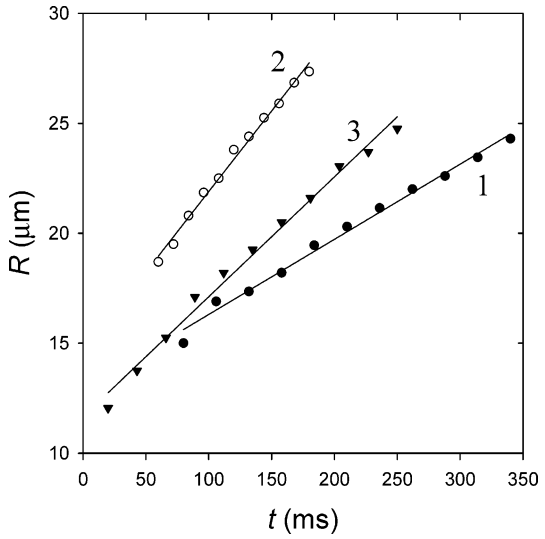

Figure 10. For the three investigated nucleation sites, rate at which the bubbles' radii, R, grow during their rise through the liquid after being released from the fiber's tip; bubbles growth rates, dR/dt, may be linked to the liquid properties and may therefore be used as a probe for indirectly measuring $\Delta c = c_L - c_B$ (see the Appendix).

nucleating elsewhere in the flute and rising in the fiber's neighborhood. In a previous work, convection induced by rising bubbles was indeed easily underscored in a glass of champagne, by following the fall of a dye drop after it struck the liquid surface.[8] Natural convection in the fiber's neighborhood is likely to forbid the growing of this boundary layer around the fiber, thus keeping it roughly constant by continuously supplying the liquid around the fiber with CO_2-dissolved molecules freshly renewed from the liquid bulk. Therefore, the mass transfer of CO_2-dissolved molecules from the liquid bulk to the gas pocket trapped inside the fiber's lumen is rather believed to be governed by diffusion−convection rather than by pure diffusion. Consequently, during the bubbling process, the boundary layer thickness around the gas pocket growing trapped inside the fiber's lumen is believed to remain reasonably constant during the growth of numerous successive gas pockets from a given fiber's lumen. Thus, $\lambda_{SC} \approx \lambda_{FW} = \lambda$.

Equation 11 may therefore be easily integrated. Strictly speaking, Δc in eq 11 is time dependent. Actually, Δc progressively decreases with time because CO_2 molecules progressively escape from the liquid medium during the bubbling process. Nevertheless, during the growth of a single gas pocket growing trapped in the fiber's lumen, Δc may also be considered as a constant. Finally, eq 11 admits a simple analytical solution, and by integrating it, the growth of a Taylor-like bubble trapped inside a fiber's lumen may be linked with both liquid and fiber parameters as

$$\begin{cases} z(t) \approx (z_0 + a\mathrm{T}) \exp(t/\mathrm{T}) - a\mathrm{T} \\ \text{with } \mathrm{T} = \dfrac{(P_0 + 2\gamma/r)r\lambda}{2\mathscr{R}\theta D_\perp \Delta c}, \text{ and } a = \dfrac{4\mathscr{R}\theta D_0 \Delta c}{(P_0 + 2\gamma/r)\lambda} \end{cases} \quad (14)$$

where z_0 is the initial length of the Taylor-like bubble before it starts its growth through the lumen, before each cycle of bubble production (see, for example, Figure 6a and j).

Three Taylor-like bubbles growing trapped inside three different fibers' lumens were investigated with the high-speed video camera. The results are reported in Figure 9, where trapped bubbles' lengths are plotted versus time during one period of the cycle of bubble production. It clearly appears from Figure 9 that the trapped bubbles' growth shows an exponential-like time dependence, as expected from the simple model of mass transfer fitted to the cellulose fiber geometry given by eq 14. The slope of each length-versus-time plot in Figure 9 enabled us to experimentally determine a characteristic time, T_{exp}, for each investigated bubble nucleation site. It is worth noting that the boundary layer thickness, λ, around each given Taylor-like bubble may finally be experimentally approached by replacing the theoretical characteristic time, T, defined in eq 14 with its experimental value and each parameter with its numerical value. The difference in CO_2-dissolved concentrations, Δc, can be indirectly accessed by retrieving a method developed in minute details in ref 9 (see the Appendix). Actually, the growth rate, k = dR/dt, at which a bubble just released from the fiber's tip expands during its rise through the liquid, was used as a probe to access Δc. This method was therefore used to access Δc for the three Taylor-like bubbles growing trapped inside the three different fibers' lumens. The various pertinent parameters of the three investigated Taylor-like bubbles growing trapped inside their corresponding fiber are listed in Table 1. It is worth noting that the thickness of the boundary layer depleted with CO_2 molecules around the three Taylor-like bubbles is reasonably comparable and in the order of 10−20 μm.

TABLE 1: Pertinent Parameters of the Three Investigated Taylor-like Bubbles Growing Trapped Inside Their Corresponding Fiber

site number	1	2	3
r (μm)	6	6	5
z_0 (μm)	22	19	27
z_f (μm)	113	80	82
T_{exp} (ms)	681	171	155
k = dR/dt (μm/s)	34	73	54
$\Delta c = c_L - c_B$ (mol/m^3)	18.0	38.6	28.5
$\lambda_{exp} \approx \dfrac{2\mathscr{R}\theta D_\perp \Delta c \mathrm{T}_{exp}}{(P_0 + 2\gamma/r)r}$ (μm)	26	14	11

4. Conclusions and Summary

The dynamics of bubble nucleation from the lumen of immersed cellulose fibers stuck on the wall of glass poured with champagne were accurately observed, in situ, from high-speed video recordings. We provided evidence that the cycle of bubble

production can be divided into two steps: (i) the growth of the gas pocket trapped inside the fiber's lumen and (ii) the bubble detachment as the gas pocket reaches the fiber's tip. With the time scale of bubble detachment being much smaller than the relative slow growth of the gas pocket, the cycle of bubble production was found to be largely governed by the growth of the gas pocket trapped inside the fiber's lumen. A model based on the diffusion of carbon dioxide molecules from the liquid bulk to the gas pocket was then developed and found to be in good agreement with our experimental data. Convection was found to play a major role in this process, and the boundary layer around the gas pocket where a gradient of dissolved gas molecules exists was indirectly approached and found to be in the order of 10−20 μm. These results directly apply to the kinetics of carbon dioxide bubble formation from glasses poured with carbonated beverages, where most of the bubble nucleation sites were recently identified as being cellulose fibers. Otherwise, because most of the particles adsorbed on the wall of a container or vessel free from any particular treatment are also believed to be cellulose fibers coming from the surrounding air, the results of this paper could be indeed extended to the more general field of nonclassical heterogeneous bubble nucleation from supersaturated liquids.

Acknowledgment. Thanks are due to the Europol'Agro institute and to the "Association Recherche Oenologie Champagne Université" for financial support and to Champagne Moët & Chandon and Pommery for their collaborative efforts.

Appendix

The general equation concerning the mass transfer of molecules from the bulk of a supersaturated liquid to a bubble surface with time is

$$\frac{dN}{dt} = KA\Delta c \tag{A1}$$

where N is the number of transferred moles of CO_2, K the mass transfer coefficient, A the bubble area, and Δc the difference in CO_2 concentration between the bulk of the liquid and the bubble surface in equilibrium with the CO_2 gas in the bubble.

Assuming the gas in the rising bubble is ideal ($P_B V = N\mathcal{R}\theta$), the number of moles of CO_2 transferred into the bubble is connected with the variation of its radius, R, with time as follows:

$$\frac{dN}{dt} = \frac{P_B}{\mathcal{R}\theta}\frac{dV}{dt} = \frac{P_B}{\mathcal{R}\theta}A\frac{dR}{dt} \tag{A2}$$

where V is the bubble volume and P_B is the pressure inside the rising bubble assumed to be equal to the atmospheric pressure, P_0, because both the hydrostatic pressure ($\rho gH < 10^{-2}P_0$) and the Laplace pressure ($2\gamma/R < 10^{-1}P_0$) inside the rising bubble are negligible.

By combining eqs A1 and A2, one obtains the rate of expansion of the bubble radius

$$\frac{dR}{dt} = \frac{\mathcal{R}\theta}{P_0}K\Delta c \tag{A3}$$

Generally speaking, heat and mass transfers are functions of two dimensionless numbers, the Sherwood and Peclet numbers, respectively, $Sh = 2KR/D_0$ and $Pe = 2RU/D_0$, with U being the velocity of ascending bubbles. In the case of small and large Pe, asymptotic solutions have been derived in the literature. Most of them are listed in the book by Sherwood et al.[19] During ascent, champagne bubbles cover a range of high Pe between approximately 10^2 and 10^5. At large Pe, Sh becomes proportional to $Pe^{1/3}$, with a numerical prefactor very close to unity. Therefore,

$$\frac{KR}{D_0} \approx \frac{2^{1/3}}{2}\left(\frac{RU}{D_0}\right)^{1/3} \Rightarrow K \approx 0.63 D_0^{2/3}\frac{U^{1/3}}{R^{2/3}} \tag{A4}$$

Combining eqs A3 and A4 leads to

$$\frac{dR}{dt} = 0.63\frac{\mathcal{R}\theta}{P_0}D_0^{2/3}\frac{U^{1/3}}{R^{2/3}}\Delta c \tag{A5}$$

By combining the empirical rising velocity, U, of ascending champagne bubbles[9] with eq A5, the rate of increase of the ascending bubble radius becomes

$$k = \frac{dR}{dt} \approx 0.63\frac{\mathcal{R}\theta}{P_0}D_0^{2/3}\left(\frac{2\epsilon\rho g}{9\eta}\right)^{1/3}\Delta c \tag{A6}$$

where ϵ is a numerical prefactor close to 0.7.

Equation A6 was found to be in very good agreement with the order of magnitude of experimental bubble growth rates in champagne and beer glasses.[8,9] Therefore, the good agreement between experimental and theoretical bubble growth rates gave us the idea to use the experimental rising bubble growth rate as a probe for measuring Δc in the liquid medium. Finally, by retrieving eq A6 in reverse order, Δc may be linked to the rising bubble growth rate, k, and some liquid parameters as follows:

$$\Delta c \approx \frac{P_0}{0.63\mathcal{R}\theta}D_0^{-2/3}\left(\frac{9\eta}{2\epsilon\rho g}\right)^{1/3}k \tag{A7}$$

Nomenclature

A	bubble area, m^2
c_B	concentration of CO_2-dissolved molecules around the gas pocket in equilibrium with the pressure of CO_2 molecules in the vapor phase inside the gas pocket (following Henry's law), mol m^{-3}
c_L	concentration of CO_2-dissolved molecules in the bulk of the supersaturated liquid medium, mol m^{-3}
Δc	difference in CO_2-dissolved concentrations between the liquid bulk, and the close vicinity of the bubble surface in equilibrium with the gaseous CO_2 into the gas pocket, $=c_L - c_B$, mol m^{-3}
D	diffusion coefficient, $m^2\ s^{-1}$
D_0	diffusion coefficient in the liquid bulk of CO_2-dissolved molecules, $m^2\ s^{-1}$
$D_\perp$	transversal diffusion coefficient of CO_2-dissolved molecules inside the fiber wall, $m^2\ s^{-1}$
e	fiber wall thickness, ≈1−5 μm
g	gravity acceleration, 9.8 m s^{-2}
h	characteristic length of a fiber, ≈100 μm
k_H	Henry's law constant
k	bubble growth rate dR/dt, m s^{-1}
k_B	Boltzman constant, 1.38×10^{-23}, J K^{-1}
K	mass transfer coefficient, m s^{-1}
N	number of moles of CO_2
P_0	atmospheric pressure, ≈10^5 N m^{-2}
P_B	pressure inside a bubble, N m^{-2}
Pe	Peclet number, $2RU/D$
r	radius of aperture of the lumen of a cellulose fiber acting as a bubble nucleation site, ≈5−10 μm
r_C	critical radius in the classical nucleation theory, $= -2\gamma/\Delta g_V$

R bubble radius, m

$\mathscr{R}$ ideal gas constant, 8.31 J K^{-1} mol^{-1}

Sh Sherwood number, $2KR/D$

t time, s

T characteristic time required for the fiber to be completely submerged by the liquid edge, s

u velocity at which the meniscus advances inside the fiber's lumen by capillary action (see Figure 3), m s^{-1}

U bubble velocity, m s^{-1}

v velocity of the liquid edge advancing over the glass wall, m s^{-1}

V bubble volume, m^3

z length of the gas pocket growing trapped inside a fiber's lumen

z_0 initial length of the gas pocket growing trapped inside a fiber's lumen

z_f final length of the gas pocket growing trapped inside a fiber's lumen, when it reaches a fiber's tip

Greek Letters

α angle of inclination of a fiber with regard to the liquid edge advancing along the glass wall when pouring

ϵ numerical prefactor in eq A6

φ contact angle between the liquid and the wall of the fiber's lumen (see Figure 3)

λ thickness of the boundary layer, m

η fluid dynamic viscosity, kg m^{-1} s^{-1}

ρ fluid density, kg m^{-3}

γ liquid surface tension, N m^{-1}

θ temperature, K

τ characteristic time required to fill the fiber's lumen by capillary rise, s

T characteristic time scale of the exponential-like bubble growth (see eq 14)

Subscripts

FW fiber wall

SC spherical cap

References and Notes

(1) Shoji, M.; Takagi, Y. *Int. J. Heat Mass Transfer* **2001**, *44*, 2763.
(2) Kornfled, M.; Suvorov, L. *J. Appl. Phys.* **1944**, *15*, 495.
(3) Tufaile, A.; Sartorelli, J.-C. *Phys. Rev. E* **2002**, *66*, 056204.
(4) Delale, C. F.; Hruby, J.; Marsik, F. *J. Chem. Phys.* **2003**, *118*, 792.
(5) Shafer, N. E.; Zare, R. N. *Phys. Today* **1991**, *44*, 48.
(6) Liger-Belair, G. *Sci. Am.* **2003**, *288* (1), 80.
(7) Liger-Belair, G. *Uncorked: The Science of Champagne*; Princeton University Press: Princeton, NJ, 2004.
(8) Liger-Belair, G. *Ann. Phys. Fr.* **2002**, *27* (4), 1.
(9) Liger-Belair, G.; Vignes-Adler, M.; Voisin, C.; Robillard, B.; Jeandet, P. *Langmuir* **2002**, *18*, 1294.
(10) Liger-Belair, G.; Topgaard, D.; Voisin, C.; Jeandet, P. *Langmuir* **2004**, *20*, 4132.
(11) Blander, M.; Katz, J. L. *AIChE J.* **1975**, *21*, 836.
(12) Lubetkin, S. D. *Langmuir* **2003**, *19*, 2575.
(13) Jones, S. F.; Evans, G. M.; Galvin, K. P. *Adv. Colloid Interface Sci.* **1999**, *80*, 27.
(14) Autret, G.; Liger-Belair, G.; Nuzillard, J.-M.; Parmentier, M.; Dubois de Montreynaud, A.; Jeandet, P.; Doan, B. T.; Beloeil, J.-C. *Anal. Chim. Acta* **2005**, *535*, 73.
(15) O'Sullivan, A. *Cellulose* **1997**, *4*, 173.
(16) Lucas, R. *Kolloid Z.* **1918**, *23*, 15.
(17) Washburn, E. W. *Phys. Rev.* **1921**, *17*, 273.
(18) Liger-Belair, G.; Prost, E.; Parmentier, M.; Jeandet, P.; Nuzillard, J.-M. *J. Agric. Food Chem.* **2003**, *51*, 7560.
(19) Sherwood, T. K.; Pigford, R. L.; Wilke, C. R. *Mass Transfer*; Chemical Engineering Series; MacGraw-Hill: 1975; Chapter 6.